Development/Plasticity/Repair

L1 Interaction with Ankyrin Regulates Mediolateral Topography in the Retinocollicular Projection

Mona Buhusi, Monika C. Schlatter, Galina P. Demyanenko, Randy Thresher, and Patricia F. Maness
Department of Biochemistry, University of North Carolina School of Medicine, Chapel Hill, North Carolina 27599

Dynamic modulation of adhesion provided by anchorage of axonal receptors with the cytoskeleton contributes to attractant or repellent responses that guide axons to topographic targets in the brain. The neural cell adhesion molecule L1 engages the spectrin-actin cytoskeleton through reversible linkage of its cytoplasmic domain to ankyrin. To investigate a role for L1 association with the cytoskeleton in topographic guidance of retinal axons to the superior colliculus, a novel mouse strain was generated by genetic knock-in that expresses an L1 point mutation (Tyr1229His) abolishing ankyrin binding. Axon tracing revealed a striking mistargeting of mutant ganglion cell axons from the ventral retina, which express high levels of ephrinB receptors, to abnormally lateral sites in the contralateral superior colliculus, where they formed multiple ectopic arborizations. These axons were compromised in extending interstitial branches in the medial direction, a normal response to the high medial to low lateral SC gradient of ephrinB1. Furthermore, ventral but not dorsal L1(Y1229H) retinal cells were impaired for ephrinB1-stimulated adhesion through β1 integrins in culture. The retinocollicular phenotype of the L1(Tyr1229His) mutant provides the first evidence that L1 regulates topographic mapping of retinal axons through adhesion mediated by linkage to the actin cytoskeleton and functional interaction with the ephrinB/EphB targeting system.

Key words: **L1; retinocollicular; ankyrin; ephrinB; axon guidance; cell adhesion**

Introduction

Navigation of axons to their synaptic targets and formation of topographic maps are orchestrated by the action of cell adhesion molecules, attractant and repellent ligands, and growth cone guidance receptors (Maness and Schachner, 2007). An important challenge is to identify functional interactions between adhesion molecules and specific guidance receptors to better comprehend the mechanism of axon targeting and map formation. The projection of retinal ganglion cell (RGC) axons to their targets in the superior colliculus (SC) to form a topographic map is the best understood axon guidance pathway. Ephrin ligands and their receptors, Eph tyrosine kinases, are pivotal axon guidance molecules specifying the retinocollicular map (Drescher et al., 1995; Birgbauer et al., 2000; Feldheim et al., 2000, 2004; Mann et al., 2004). Countergradients of A-class ephrins in the SC and their EphA receptors on RGC axons contribute to mapping of axons from the temporonasal axis of the retina to coordinates along the anteroposterior axis of the SC, whereas countergradients of B-class ephrins in the SC and their ephrinB (EphB) receptors on RGC axons map the dorsoventral axis of the retina to the mediolateral axis of the SC (Lemke and Reber, 2005; McLaughlin and O'Leary, 2005; Flanagan, 2006). Depending on their concentration, ephrins can exert both positive and negative effects on axon growth, ranging from complete inhibition to growth promotion (Hansen et al., 2004), so that the final map position of an axon terminal is the point where positive and negative forces balance out (Flanagan, 2006). However, this model does not fully account for the retinocollicular map, as the phenotypes of animals with ephrin or Eph loss-of-function mutations are not fully penetrant. Previous studies show that Wnt/Ryk signaling is another contributor to mediolateral targeting of RGC axons providing a counterbalancing force in ephrinB-mediated medial attraction (Schmitt et al., 2006) and other modulators are still to be uncovered.

L1 is a neural cell adhesion molecule expressed on developing retinal axons and their growth cones, known to participate in retinocollicular guidance. In L1 deficient mice, temporal retinal axons exhibit targeting defects along the anteroposterior axis of the SC (Demyanenko and Maness, 2003), similar to Ephrin A2/A5 null mutants (Feldheim et al., 2000), although targeting along the mediolateral axis is affected to a lesser extent. Thus, L1 might interact functionally with EphA and EphB receptors to control retinal axon targeting along both axes, providing the adhesion force needed for guidance.

Attractant and repellent axon guidance is regulated by dynamics in the actin and microtubule cytoskeleton, which may influence adhesion (Kalil and Dent, 2005). L1 is able to serve as a mechanical integrator of traction forces at the membrane through anchorage to the actin cytoskeleton (Gil et al., 2003). L1 cooperate with β1 integrins in potentiating cell adhesion and migration (Felding-Habermann et al., 1997; Silletti et al., 2000; Thelen et al., 2002; Panicker et al., 2006). The extracellular do-

Received Aug. 6, 2007; revised Sept. 25, 2007; accepted Oct. 22, 2007.

This work was supported by National Science Foundation Grants 0618176, National Institutes of Health Grant R0149109, and Postdoctoral Fellowships from the Swiss National Science Foundation and Roche Research Foundation (M.C.S.). We are grateful to Dr. Elena Pasquale for helpful discussions.

Correspondence should be addressed to Patricia F. Maness, Department of Biochemistry, University of North Carolina School of Medicine, CB 7260, Chapel Hill, NC 27599. E-mail: srclab@med.unc.edu.

M. Buhusi's present address: Department of Neurosciences, Medical University of South Carolina, Charleston, SC 29425.

DOI:10.1523/JNEUROSCI.3573-07.2008

 0270-6474/08/280177-12$15.00/0

main of L1 can mediate cell-to-matrix or cell-to-cell adhesion through *cis*-interactions with β1-integrins or *trans* homophilic binding, whereas the L1 cytoplasmic domain can stabilize adhesive interactions by transmitting force from the membrane to the cell through its ability to link to the cytoskeleton. Indeed, the L1 cytoplasmic domain provides linkage to the actin cytoskeleton through ankyrin and ezrin-radixin-moesin binding (Dickson et al., 2002). A conserved sequence in the cytoplasmic domain of L1 cell adhesion molecules (L1CAMs) (SFIGQY) reversibly binds ankyrin, a spectrin adapter that couples L1 to the subcortical actin cytoskeleton (Davis and Bennett, 1994). L1CAM linkage to ankyrin is modulated by phosphorylation on the tyrosine ^{1229} residue of the SFIGQY motif by an unknown kinase (Jenkins et al., 2001). A mutation of tyrosine 1229 to histidine interferes with ankyrin binding (Needham et al., 2001). The importance L1–ankyrin binding in human neurodevelopment is underscored by the fact that the Y1229H mutation in L1 is a pathological mutation underlying the L1 syndrome of mental retardation (Kenwrick et al., 2000).

To probe the role of L1 anchorage to the cytoskeleton in axonal guidance *in vivo*, we generated a novel mouse line in which the *L1cam* gene was replaced with the L1(Y1229H) mutation by genetic knock-in. Analysis of the retinocollicular map of L1(Y1229H) mutant mice revealed a phenotype with striking mediolateral mapping errors and misdirected interstitial branching of RGC axons. This phenotype was different from that of the L1 total knock-out (Demyanenko and Maness, 2003), and strikingly resembled the map of EphB2/EphB3-deficient mice (Hindges et al., 2002). Loss of ankyrin binding resulted in decreased integrin-dependent adhesion and ephrinB1 responsiveness in ventral but not dorsal retinal cells in culture, correlating with EphB receptor expression. The retinocollicular phenotype of the L1(Y1229H) mutant mice provides the first example of a point mutation in an adhesion molecule that disrupts topographic axon targeting.

Materials and Methods

All animals were used according to University of North Carolina at Chapel Hill Institutional Animal Care and Use Committee policies and in accordance with National Institutes of Health guidelines.

Generation of L1(Y1229H) mutant mice. The genomic sequence of the mouse L1 gene was obtained from BACs (bacterial artificial chromosomes) 309B4 and 567G9 from a 129Sv embryonic stem (ES) cell library (a gift from Dr. Gaiping Wen, Institute for Molecular Biology, Jena, Germany). A fragment (1.6 kb) containing exon 28 encoding part of the L1 cytoplasmic domain together with the 3′ untranslated region of the mouse L1 gene was transferred to pBluescript (Stratagene, La Jolla, CA) and modified by Quikchange mutagenesis using the following primers: Y1229H-FP, 5′-TTTCATCGGCCAGCACTCGGGCAAGAAAGAGAAGGAGGC-3′ and Y1229H-RP 5′-GCCTCCTTCTCTTTCTTGCCCGAGTGCTGGCCGATGAAAG-3′. The mutation was confirmed by sequencing and the 3′ L1 fragment was transferred to a targeting vector (OS dup/del; University of North Carolina Animal Models Facility). Another fragment (5.6 kb) of the mouse L1 genomic sequence consisting of exons 15–27 was also inserted into this plasmid to serve as the 5′ arm of homology (see Fig. 1*A*). The plasmid was electroporated into ES cells, which were further cultured under G418 selection medium. Three hundred clones were analyzed for homologous recombination by PCR and two PCR-positive clones were confirmed using Southern blotting. For PCR screening, we used a forward primer in 3′ region of the L1 genomic sequence, outside the fragment used for targeting (5′-GATAACATGACATCAGGTACAACATACAGG-3′) and a reverse primer in the neomycin resistance gene (5′-CTATTCGGCTATGACTGGGCACAACAG-3′). For Southern analysis, genomic DNA from the PCR-positive clones was digested with *Xba*I and *Pac*I (site introduced through recombination), and a radioactively labeled probe (exons 16–19) was used to detect the fragment corresponding to the L1 sequence. This probe detected a wild-type (WT) band of 10 kb in parental ES cells and a targeted (neomycin+) band of 7 kb in the PCR-positive clones (see Fig. 1*C*). In a second step, the neomycin-resistance gene in intron 27 was eliminated from the genomic DNA by *cre*-mediated recombination in ES cells, and selected clones were retested by Southern blotting and allele-specific PCR (using primers that recognize either the WT or the mutant sequence in exon 28: EX28WT 5′-TCTTTCATCGGCCAGCACTCG-3′ and EX28MUT 5′-CTCTTTCATCGGCCAGTACAG-3′, and a primer annealing to a sequence in intron 27 ACROSSL1RP 5′-AATAAAGAGGGTAGCGGGTGGTAAG-3′) (see Fig. 1*B*). The WT set of primers amplified a 450 bp fragment from only the parental ES cells, whereas the MUT set of primers amplified a 1600 bp fragment from the neomycin-positive mutant clone and a 550 bp from the final neomycin-negative clone, and did not anneal to the parental ES cell DNA. A PCR using primers on both sides of the neomycin cassette (AcrossL1FP in the 3′ region of the L1 gene and AcrossL1RP in intron 27) confirmed the excision of the neomycin cassette (see Fig. 1*B*) by *cre* recombination. After the *cre*-mediated excision of the neomycin gene, the Southern blot probe recognized a targeted (neomycin−) band of ~6 kb (see Fig. 1*C*).

Mouse blastocysts were injected with six different selected ES clones and transferred to pseudopregnant mice in the University of North Carolina Animal Models Facility. Fifteen chimeric male mice were obtained, four of which demonstrated germline transmission. Male chimeras were mated with WT 129S1/SvImJ mice to generate isogenic L1(Y1229H) heterozygous females. After genotyping female offspring by allele-specific PCR (see Fig. 1*D*), the L1(Y1229H) heterozygotes were mated to WT males to obtain male L1 mutants [L1(Y1229H)/Y; 50% of male offspring] and control littermates for analysis. To show whether genetic background influences phenotype, heterozygous females were backcrossed to C57BL/6J to create a nearly congenic line. L1(Y1229H) mutant males were obtained at the expected Mendelian ratio, indicating that the mutation does not induce embryonic lethality. Mutant males were long lived and fertile in 129S1/SvImJ inbred and 129S1/SvImJ by C57BL/6J mixed backgrounds.

Axon tracing and analysis. Axonal tracing was performed essentially as described previously (Simon and O'Leary, 1992; Demyanenko and Maness, 2003). L1(Y1229H) mutant males and WT littermates at P2–P3 and P10–P12 were anesthetized and anterograde tracing was performed by focal injection of DiI (Invitrogen, Carlsbad, CA) as an 10% solution in dimethylformamide or dimethylsulfoxide into the peripheral region of the retina using a Picospritzer II (General Valve, Fairfield, NJ) and capillary glass micropipettes (tip internal diameter, ~40 μm). After 48 h, mice were deeply anesthetized and perfused transcardially with 4% paraformaldehyde in 0.1 M phosphate buffer (PB), pH 7.4. Before removing the retina, the eye was visually inspected to identify the injection site and assess its position in the required quadrant relative to the extraocular muscles (lateral and inferior recti). The eyes were then removed and incisions were made to demarcate the four quadrants of the retina. To verify the injection sites and analyze the projection areas, injected retinas as well as superior and inferior colliculi were whole-mounted onto glass slides and examined by epifluorescence and confocal microscopy (University of North Carolina Microscopy Services; LSM 5; Zeiss, Oberkochen, Germany) using appropriate filters. The injection sites covered 3–5% of the retina. The boundaries of the SC and IC were determined by their characteristic shape and location. Termination zones (TZs) were verified by their branched appearance at high magnification. For analysis, images of the SC were acquired at the same magnification, and the locations of the TZs were scored along the mediolateral (x) and anteroposterior (y) axes. The anteromedial corner of the SC was considered as the zero point ($x = 0$; $y = 0$).

To quantitatively evaluate branch orientation of ventrotemporal (VT) axons in L1(Y1229H) and WT mice at P2–P3, the SC was divided into three bins along the mediolateral axis, relative to the emerging TZ: lateral to TZ, within TZ, and medial to TZ, as described previously (Hindges et al., 2002). Only mutants with one normally positioned TZs were included in this analysis. The total number of labeled axons and branches was counted in confocal z-stacks, and medial or lateral branch orientation was recorded for each bin. The results were expressed as a directional

coefficient (DC), which was a ratio calculated for each subject in each of the three SC bins as the difference in medial and lateral branches divided by the total number of branches. A positive DC indicated more medial than lateral branches, whereas a negative DC indicated more lateral than medial branches. The directional coefficients were compared by a mixed ANOVA for WT and L1(Y1229H) mutant genotypes.

To evaluate the distribution of DiI-labeled VT axons entering the SC at P2–P3, after retinal injections at P1, the entrance zone into the SC was divided in 10 equal bins, four medial to TZ and six lateral to TZ as in (Hindges et al., 2002). The percentage of axons entering the SC in each bin was scored for each subject, and then averaged over groups. The distribution of axons (expressed as percentage of total for each bin) for WT and L1(Y1229H) mice was analyzed by a mixed ANOVA.

For measurements of the optic nerve, chiasm, and optic tract, DiI crystals were applied using the tip of a needle to the optic disc of one eye to label a maximum number of contralaterally and ipsilaterally projecting axons in L1(Y1229H) and WT mice (P10) after perfusion with 4% paraformaldehyde. Brains were stored at 37°C for 4–6 weeks to allow diffusion. The optic nerves and chiasm were whole-mounted onto glass slides and imaged under epifluorescence microscopy. NIH ImageJ software was used for measurement of the diameter of the optic nerve taken 400 μm from the midline of the chiasm, the width of the optic chiasm at the midline, and the width of the contralateral and ipsilateral optic tract taken 100 μm from the midline of the optic chiasm. Differences in means for WT and L1(Y1229H) mice were calculated by the two-tailed t test ($p \leq 0.05$).

Immunofluorescence and Nissl staining. Postnatal mice (P0, P3, and P8) were deeply anesthetized by hypothermia (P0) or isoflurane (P3–P8) and perfused transcardially with phosphate buffer (PB), followed by 4% paraformaldehyde in PB. Brains or entire heads were collected and post-fixed for at least 24 h at 4°C in 4% paraformaldehyde in PB. Samples were cryoprotected in 30% sucrose in PBS at 4°C for 48 h, then embedded in Tissue-Tek OCT and stored at −80°C. Cryostat sections (20 μm) were washed in PBS, blocked, and permeabilized with 0.2% Triton X-100, 10% donkey serum, 0.5% fish skin gelatin in PBS. Sections were incubated with primary antibodies (rat anti-L1 MAB, 1:200, Millipore, Temecula, CA; mouse anti-ankyrinB, 1:200; Invitrogen) in blocking solution overnight at 4°C, then washed in PBS with 0.05% Tween 20. Sections were incubated for 1 h with fluorescein-conjugated donkey anti-rat (L1) and Cy5-conjugated donkey anti-mouse (ankyrin) secondary antibodies (1:100; Jackson ImmunoResearch, West Grove, PA), then washed in PBS, 0.05% Tween 20, and protected with ProLong Gold (Invitrogen). Control sections were incubated with secondary antibodies only. For Nissl staining, sections were incubated with red fluorescent Nissl stain (1:150 in PBS; Invitrogen) for 10 min at room temperature, then washed for 1 h in PBS with 0.05% Tween 20. Images were taken on a Fluoview500 Olympus (Tokyo, Japan) confocal microscope using appropriate band-pass filters for FITC, tetramethylrhodamine isothiocyanate, and Cy5 (sequential scan).

Immunoblotting and immunoprecipitation. Mouse brains (P3) were collected in liquid nitrogen and lysed on ice in RIPA buffer with Halt protease inhibitor mixture (Pierce, Rockford, IL) and 1 mM phenylmethylsulfonyl fluoride. Lysates were passed through a 27G needle and then clarified by centrifugation at 14,000 × g for 20 min at 4°C. Protein concentration was determined using the bicinchoninic acid (BCA) assay (Pierce), and then equal amounts of proteins in brain lysates were separated by SDS-PAGE on 4–15% acrylamide gradient gels (Biorad, Hercules, CA) and transferred to nitrocellulose (OptiTran; Schleicher and Schuell, Keene, NH). After blocking, L1 was identified using mouse L1 antibody 2C2 (Abcam, Cambridge, MA) and a horseradish peroxidase-conjugated goat anti-mouse IgG (Jackson ImmunoResearch). Immune complexes were visualized using enhanced chemiluminescence (ECL) (Pierce).

For coimmunoprecipitation of L1 and ankyrinB, P8 SCs were frozen in liquid nitrogen and lysed in lysis buffer (20 mM Tris-HCl pH 7.4, 150 mM NaCl, 5 mM EDTA, 2 mM EGTA, 10 mM NaF, 1% Triton X-100, Halt protease inhibitor mixture, 1 mM phenylmethylsulfonyl fluoride). Equal amounts of protein in 1 ml lysis buffer were precleared with protein G-Sepharose (GE Healthcare, Piscataway, NJ) for 30 min at 4°C. Precleared lysates were incubated with L1 monoclonal antibodies 2C2 (2.5 μl) and 5G3 (2.5 μl; BD Bioscience, San Jose, CA) for 1 h at 4°C before addition of protein G-Sepharose and incubation for 30 min at 4°C. Samples were washed with ice-cold lysis buffer and analyzed by Western blotting. After blocking with 5% dry milk in TBST, the nitrocellulose was incubated with ankyrinB monoclonal antibody (1:200) for 2 h, followed by HRP-conjugated anti-mouse antibody (1:5000) for 1 h at room temperature. After ECL detection, blots were stripped and reprobed with L1 antibody 2C2 (2 μg/ml, 1 h) and HRP-conjugated goat anti-mouse secondary antibody.

Retinal cell adhesion assays. Dorsal and ventral halves of retinas of WT and L1(Y1229H) mutant mice (P3) were collected in complete HBSS, centrifuged and incubated with 1 ml of papain (10 U/ml), 200 μg L-cysteine, and 0.04% DNase at 37°C for 15 min. Samples were triturated, cells collected by centrifugation and resuspended in retinal cell medium (Neurobasal medium, 1 mM sodium pyruvate, 1 mM L-glutamine including B27, N2 supplements, and antibiotics). Cells were seeded at 50,000 cells/well in 500 μl retinal cell medium with 0.5 μl/ml brain-derived neurotrophic factor (Promega, Madison, WI) and treated with human ephrinB1-Fc fusion protein (R&D Systems, Minneapolis, MN; 1 μg/ml) preclustered with 0.2 μg/ml goat anti-human Fc antibody (Jackson ImmunoResearch) for 30 min on ice or human IgG as a control (1 μg/ml, preclustered as ephrinB1-Fc). In some experiments, 5 μg/ml echistatin (Bachem, Torrance, CA) in PBS was added to the cells. For plating, 24-well dishes were incubated with 100 μl of nitrocellulose solution (1 cm^2 in 100 ml MeOH) for 30 min at room temperature, washed with water, and incubated with 3 μg/ml fibronectin (Invitrogen) in PBS at 4°C overnight. Wells were blocked with 1% bovine serum albumin in PBS for 1 h at 37°C. After a 24 h incubation, nonadherent cells were removed by washing with PBS, and adherent cells were fixed with 4% paraformaldehyde for 20 min. Cell nuclei were stained with bisbenzimide and labeled cells were scored in 10 randomly selected fields per well under epifluorescence illumination using a 20× objective of a Zeiss Axiovert 200 microscope. Samples were performed in duplicate, and each experiment was repeated at least four times. Cell numbers were averaged and results were expressed as cells/field ±SE. Statistical significance was examined using a two-tailed t test ($p \leq 0.05$).

Results

Generation and characterization of L1(Y1229H) mutant mice

To investigate the physiological role of L1–ankyrin association in retinocollicular mapping, mice were engineered to carry a targeted mutation (Y1229H) in the ankyrin-binding site of L1 ($FIGQY^{1229}$) (Fig. 1*A*). The mutation was introduced through homologous recombination in mouse ES cells by replacing WT exon 28, encoding part of the cytoplasmic domain of the L1 gene on the X chromosome with an altered exon 28, in which the codon for tyrosine 1229 was replaced with a codon corresponding to histidine through site-directed mutagenesis. To assess recombination, selected ES cells were screened by PCR (Fig. 1*B*) and Southern blotting (Fig. 1*C*). Before injecting into mouse blastocysts, the neomycin resistance cassette in intron 27 was removed using *cre*-directed recombination in ES cells (Fig. 1*B*,*C*). Blastocyst injections of 6 different ES clones generated 15 chimeric male mice, four of which demonstrated germline transmission of the mutation. L1(Y1229H) heterozygote females were mated to WT males to obtain hemizygous mutant and WT male littermates for analysis. Genotyping was done by PCR using allele-specific amplification (Fig. 1*D*). L1(Y1229H) mutant males were obtained at the expected Mendelian ratio, indicating that the mutation did not induce embryonic lethality. Mutant males derived from four initial founder males showed similar defects in retinocollicular mapping, indicating that these defects were a result of the induced mutation. Mutant males were long lived and fertile in 129S1/SvImJ inbred and 129S1/SvImJ by C57BL/6J mixed background.

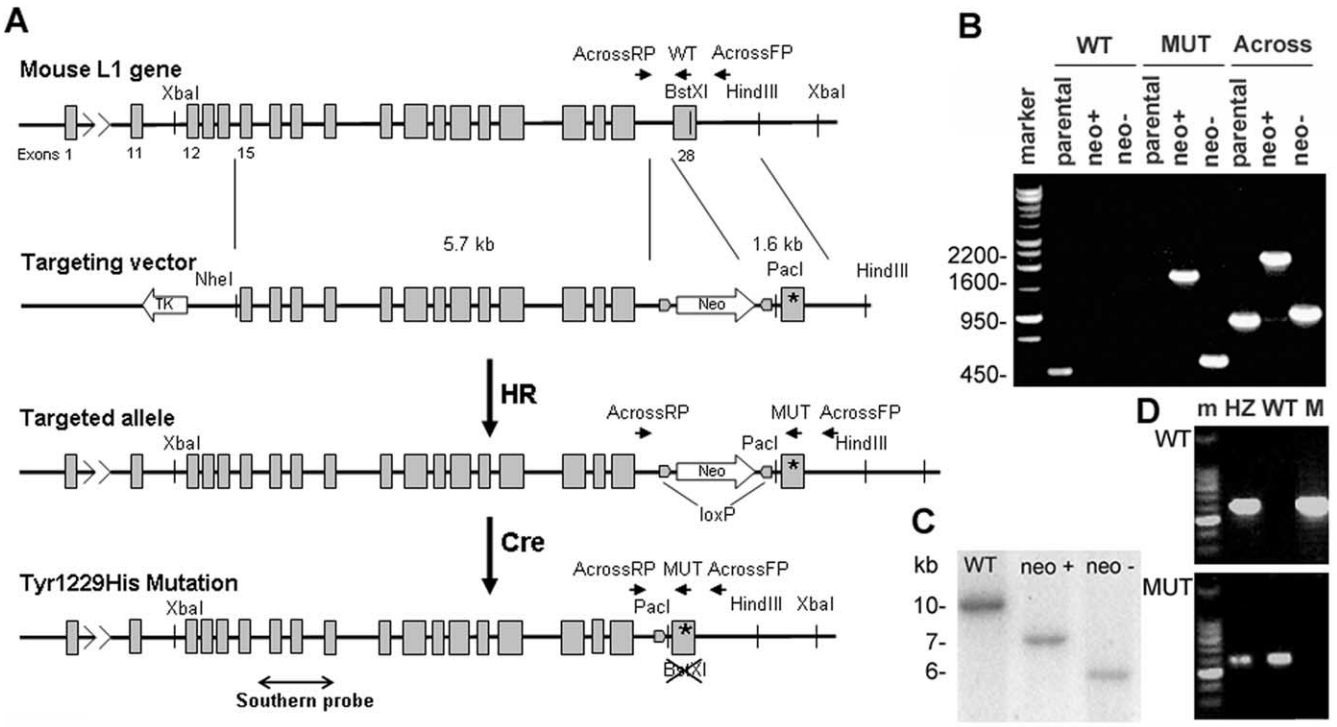

Figure 1. Generation of the L1(Y1229H) knock-in mouse. ***A***, Schematic representation of the genetic modification at the L1 locus: wild-type exon 28 was replaced by a modified exon 28 in which the codon corresponding to 1229Tyr was changed to encode His by homologous recombination (HR) in ES cells; the neomycin-resistance gene introduced at the same time in intron 27, was subsequently removed by *cre*-mediated recombination in ES cells (Cre). ***B***, PCR analysis of ES clones (parental ES cells, neomycin-positive clone after HR, neomycin-negative clone after *cre* recombination; marker, 1 kb DNA ladder). Lanes 1–3, PCR for the wild-type allele, using the WT and AcrossL1RP primers. Lanes 4–6, PCR for the mutant allele, using the MUT and AcrossL1RP primers. Lanes 7–9, PCR covering the region modified by recombination, using the AcrossL1 FP and RP primers. ***C***, Southern blot screening of recombined neomycin-positive clones and neomycin-negative clones after cutting with *Xba*I and *Pac*I (site introduced through recombination), using a probe corresponding to exons 16–19. ***D***, Mouse genotyping by PCR using allele specific primers: top row, MUT and AcrossL1RP; bottom row, WT and AcrossL1RP; m, marker (100 bp DNA ladder); HZ, heterozygote female; WT, wild-type male; M, hemizygous L1YH.

Nissl staining of L1(Y1229H) mutant brain revealed no gross neuroanatomical abnormalities compared with WT littermates. Mutant and WT brains showed a similar size and morphology of the superior colliculus, neocortex, hippocampus, thalamus (P21; Fig. 2*A*), and cerebellum as well as major axon tracts including the corpus callosum (data not shown). In contrast to L1(Y1229H) mutants, L1 total knock-out mice exhibit ventricular enlargement, agenesis of the corpus callosum, and a reduced hippocampal size (Demyanenko et al., 1999). Furthermore, L1(Y1229H) mutants displayed normal eye structure and retinal architecture with all layers present (Fig. 2*D*). The mutant L1(Y1229H) protein was expressed at similar levels to WT L1 in mouse brain (P3) relative to actin as control, and had the same intact molecular size (200–220 kDa) together with a 80 kDa cleavage fragment, which was previously described (Burgoon et al., 1991).

Ankyrin B is a major brain protein expressed as two alternatively spliced isoforms of 220 kDa and 440 kDa during retinocollicular targeting (Kunimoto et al., 1991; Otto et al., 1991; Chan et al., 1993). 220 kDa Ankyrin B is the major isoform in adult brain, whereas the 440 kDa isoform is maximally expressed in developing brain. Immunoblotting with ankyrinB antibodies showed prominent expression of 220 kDa ankyrin in WT SC at P8 (Fig. 2*C*). Immunoprecipitation of L1 from SC extracts showed that ankyrin B coimmunoprecipitated selectively with WT L1 and not with L1(Y1229H) (Fig. 2*C*). Reprobing blots with L1 antibodies confirmed that equal amounts of L1 were present in the immunoprecipitates. Because the ankyrin B antibody preferentially recognizes ankyrin B 220 kDa (Scotland et al., 1998) and antibodies recognizing the 440 kDa isoform are not available, it is not excluded that L1 might also associate with the 440 kDa ankyrinB isoform. These results established that the L1(Y1229H) mutation disrupted L1 association with ankyrin B in postnatal mouse SC.

Colocalization of L1 and ankyrin B in the developing retinocollicular pathway

Retinocollicular axon targeting in the mouse develops from E14, when RGC axons first reach the anterior border of the SC, to P10 when topographic mapping is largely complete (Simon and O'Leary, 1992). Further refinement of the map as a result of retinal activity occurs after eye opening around P12 (Schmidt, 2004). Immunofluorescence staining showed that WT and mutant L1(Y1229H) proteins were expressed in the developing retina from E17 to P8. As shown at P0, WT and mutant L1 proteins localized to the nerve fiber layer and inner plexiform layer of the retina, and in the optic nerve (Fig. 2*D*,*E*). Immunoreactivity of each protein appeared relatively uniform across both the dorsoventral and temporonasal axis of the retina, as reported for L1 (Demyanenko and Maness, 2003). WT and mutant L1 proteins were coexpressed with ankyrinB in the developing retina from E17 to P8, where they colocalized in the optic nerve, nerve fiber layer, and inner plexiform layer (P0) (Fig. 2*D*,*E*). No ankyrinB immunofluorescence was observed in RGC bodies, indicating its preferential localization to axons, but some staining in radially oriented fibers in the retina suggested its presence in Muller glial fibers. In the SC (P0–P8), L1 immunoreactivity was present in incoming RGC axons located in the optic fiber layer (P0) (Fig. 2*E*) and in axons of nonretinal origin in the deeper layers of the

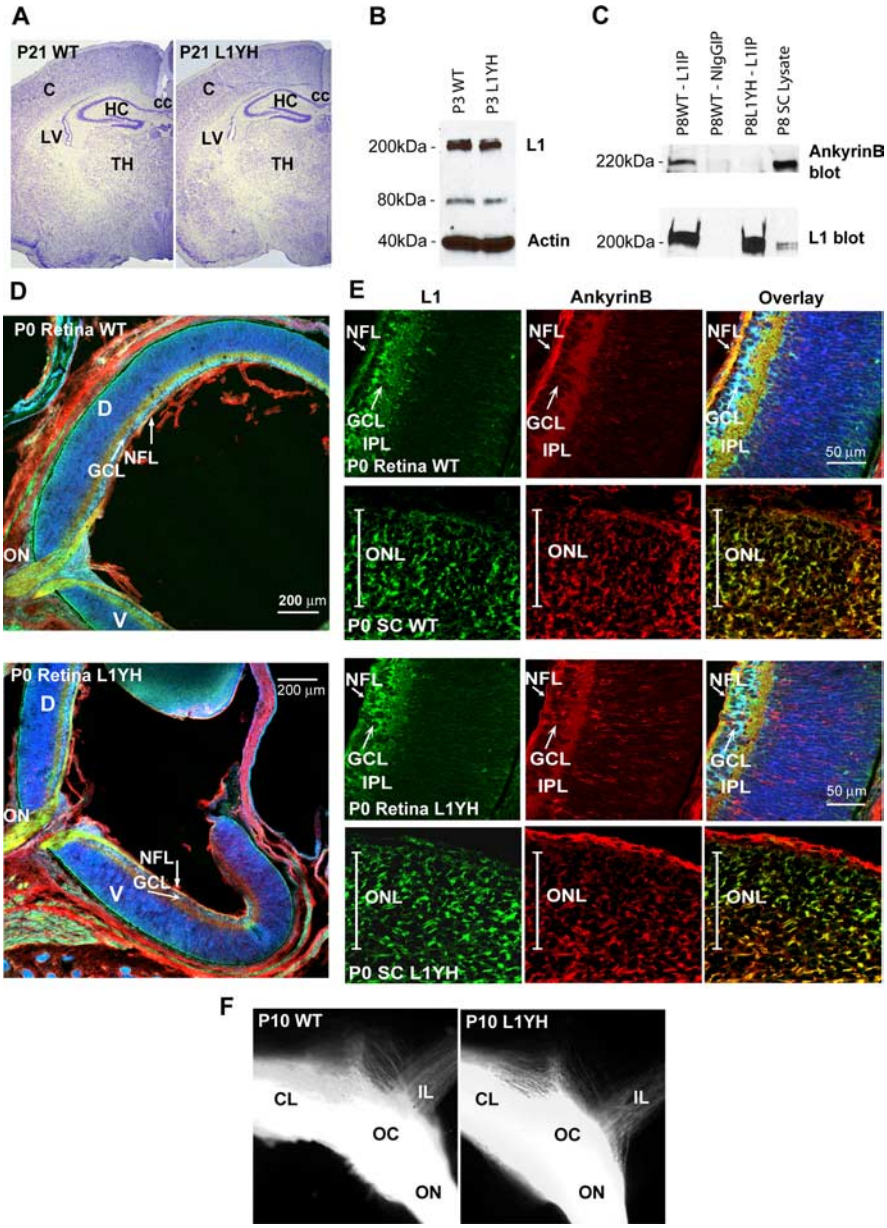

Figure 2. L1 expression and colocalization with ankyrinB in brain and retina of WT and L1(Y1229H) mice. ***A***, Nissl staining of WT and L1(Y1229H) mice at P21 (strain 129). C, Cortex; HC, hippocampus; TH, thalamus; LV, lateral ventricle; cc, corpus callosum. ***B***, Western blot analysis of P3 brain lysates (45 μg) from WT (lane 1) and mutant (lane 2) mice using an L1 antibody. ***C***, Coimmunoprecipitation of ankyrinB with L1 from WT mouse superior colliculus lysates (P8). No ankyrinB coimmunoprecipitated with nonimmune mouse IgG or with L1(Y12229H) protein. ***D***, Immunofluorescence localization of L1 and ankyrinB in sagittal sections of the P0 mouse retina. ***E***, Localization of L1 and ankyrinB in sagittal sections of the P0 mouse retina (high magnification) and in coronal sections of the superior colliculus in the anterior third of the anteroposterior axis: L1, green; ankyrinB, red; Nissl stain, pseudocolored blue. NFL, Nerve fiber layer; GCL, ganglion cell layer; IPL, inner plexiform layer; D, dorsal; V, ventral; ON, optic nerve; ONL, optic nerve layer in the SC. ***F***, Optic chiasm visualized by DiI tracing from the left retina. Contralateral (CL) and ipsilateral (IL) projections in WT and L1(Y1229H) littermates were of similar sizes.

SC (asterisk) (Lyckman et al., 2000). AnkyrinB colocalized with L1 in axons at these locations (Fig. 2*E*, overlay) and appeared uniform across the lateromedial axis of the SC. L1(Y1229H) showed a similar distribution and colocalization with ankyrinB in the SC (Fig. 2*E*, overlay).

Countergradients of EphB receptors along the dorsoventral axis of the retina (high ventral to low dorsal) and ephrinB1 along the mediolateral axis of the SC (high medial to low lateral) establish topographically appropriate projections across the mediolateral SC axis (Hindges et al., 2002). EphrinB/EphB interactions during retinocollicular mapping do not result in an inhibitory, repellent response of growth cones, but instead appear to mediate attraction of interstitial axon branches up the ephrinB1 gradient of the SC (Hindges et al., 2002). L1(Y1229H) mutant mice (P0) showed no difference in the level or pattern of immunofluorescence staining of EphB2 in the retina or ephrinB1 in the SC compared with WT (data not shown), with the same graded pattern as reported previously (Hindges et al., 2002).

Retinotopic mapping defects in L1(Y1229H) mice

L1 knock-out mice show major defects in targeting of temporal RGC axons along the anteroposterior axis, resulting in overshooting the correct TZ as well as lateral displacement (Demyanenko and Maness, 2003). To investigate the effects of disrupting the L1–ankyrin interaction on axonal growth and guidance, the topographic projections of RGC axons in the SC of L1(Y1229H) mice were analyzed at stages when the basic topography of the retinocollicular map resembles its mature form (P10–P12). Focal injections of the axonal tracer DiI were made into the retina of live, anesthetized mice at P8–P10, and labeled RGC projections in the SC were analyzed 2 d later. Analyses were restricted to animals in which retinal whole mounts displayed a single DiI injection of appropriate size (3–5% of the retina) and positioning relative to the insertions of the extraocular muscles.

During development of the topographic map, temporal RGC axons project to the contralateral SC, whereas nasal axons project to the posterior SC by mechanisms requiring ephrinA/EphA receptor signaling (Feldheim et al., 2000, 2004). Thus, altered anteroposterior mapping is most evident in the projection of temporal axons, although deviation along the mediolateral axis would also be observed. As expected, in 10 of 10 WT mice focal DiI injections into the midtemporal (T) retina labeled a single dense TZ in the middle anterior region of the contralateral SC (Fig. 3*A*,*B*). In contrast, similar injections into the mid-temporal retina of L1(Y1229H) mutants identified topographic targeting errors along the mediolateral axis of the contralateral SC. In 22 of 28 injections, mutant axons terminated at abnormally lateral sites, mostly as multiple ectopic termination zones (eTZs) that appeared to be connected to a correct TZ in the midanterior SC (8 of 28 cases) (Fig. 3*D–F*). Alternatively, mutant temporal axons terminated as a single laterally displaced TZ (14 of 28 cases) (Fig. 3*G*). The percentage of cases with abnormal mediolateral positioning in the mutant mice was significantly different from WT ($\chi^2 = 18.66$; $p < 0.0001$) (Fig. 4). In mutants,

TZs or eTZs were often slightly malpositioned posteriorly along the anteroposterior axis of the SC (Figs. 3*F*,*G*, 4) but not to the same extent seen in L1 null mutant mice (Demyanenko and Maness, 2003). To more critically assess the mediolateral misplacement of TZs in mutant mice, VT retinal injections of DiI were performed in mutants and WT littermates. Because VT axons express high levels of EphB receptors and normally project to the anteromedial corner of the SC, their attractive response to the high medial to low lateral ephrinB1 gradient in the SC renders them especially sensitive to deficiencies in mediolateral targeting, which is regulated by ephrinB1/EphB receptor signaling (Hindges et al., 2002). In seven of seven WT mice, VT retinal injections resulted in labeling a single well defined TZ in the anteromedial SC (Fig. 3*H*,*I*). In contrast, VT axons of 10/15 mutants projected to abnormally lateral SC sites (Fig. 3*J–L*). In 8 of 15 cases, mutant VT axons formed multiple ectopic TZs in addition to a correctly positioned TZ, whereas in 2 of 15 cases a single laterally displaced TZ was observed. The percentage of cases with abnormal targeting of VT axons in L1(Y1229H) mutant mice was significantly different from WT ($\chi 2 = 8.55$; $p < 0.005$) (Fig. 4). VT axons of L1(Y1229H) mice rarely terminated posteriorly along the anteroposterior SC axis, indicating that L1–ankyrin interactions play a more significant role in mediolateral rather than anteroposterior targeting of these axons.

The projection of RGC axons from the dorsal or nasal retina was not perturbed in L1(Y1229H) mutants. Dorsal retinal injections in L1(Y1229H) mice resulted in labeling of a single TZ within the lateral SC located midway along the rostrocaudal axis (Fig. 3*O*,*P*) ($n = 2$), which occurred at the same location in WT mice (data not shown). Nasal retinal injections in L1(Y1229H) mice resulted in labeling of a single TZ in the mid-posterior SC ($n = 8$) (Fig. 3*M*,*N*) at the same location as in WT mice (data not shown). Thus, mapping of RGC axons from the dorsal and nasal retina appeared to be relatively unaffected by the ankyrin binding site mutation in L1. It should be added that immunofluorescence staining for EphB2 in the retina and ephrinB1 in the SC of L1(Y1229H) and WT mice (P0) showed no differences in level of expression (data not shown).

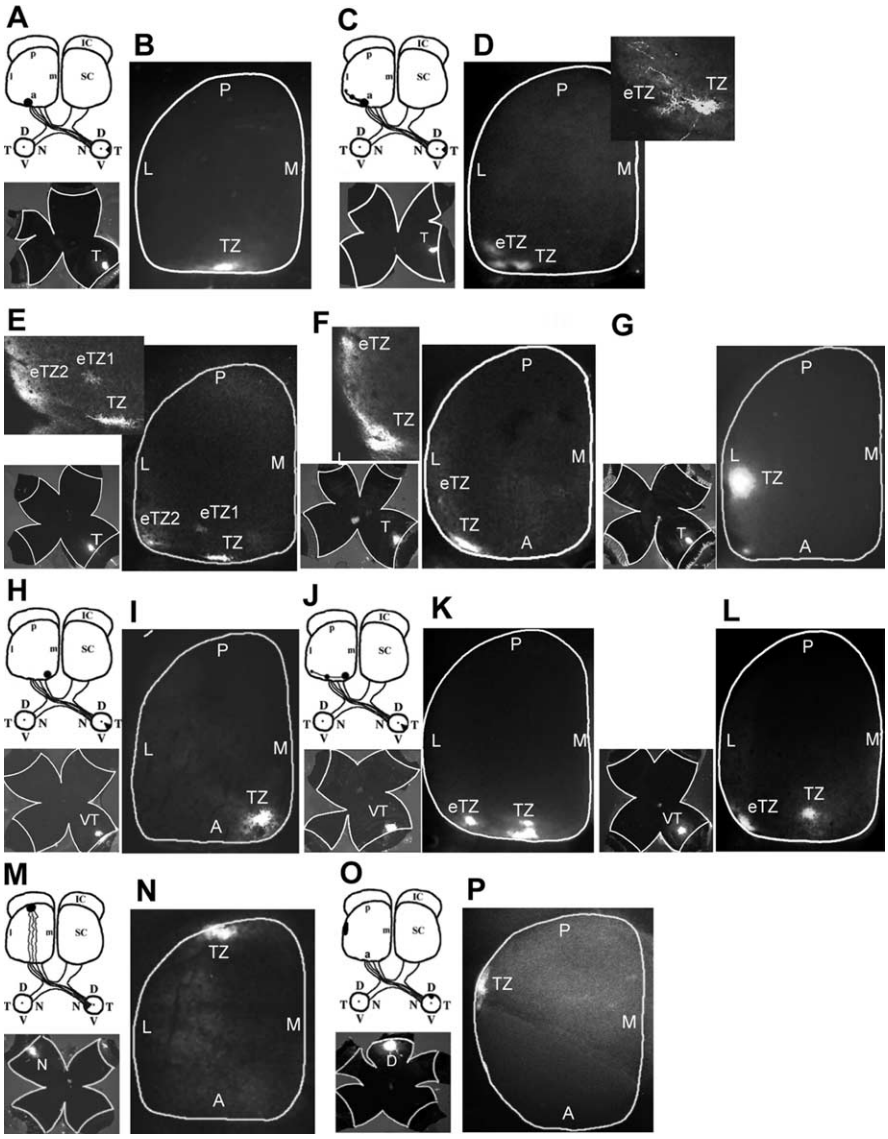

Figure 3. Defects in retinocollicular mapping in L1(Y1229H) mutant mice. ***A***, ***B***, Injection of DiI into the peripheral temporal retina (shown in flatmount) at P8 labeled a single TZ in the anterior SC in P10 WT mice. ***C–G***, DiI injections in the peripheral temporal retina of L1(Y1229H) mutant mice revealed ectopic TZs (eTZ), displaced to lateral and slightly posterior positions in the SC. ***D–F***, Higher magnification of the TZs (top left) revealed branches extending laterally or posteriorly toward the eTZs. ***H***, ***I***, Focal injections of DiI in the ventrotemporal (VT) retina labeled a single dense TZ in the anteromedial corner of the SC in P10 WT mice. ***J–L***, Similar injections in L1(Y1229H) mutant mice resulted in eTZs displaced laterally within the anterior SC. ***M***, ***N***, Nasal retinal injections in L1(Y1229H) mutant mice resulted in labeling of a single TZ in the posterior SC at P10. ***O***, ***P***, Injection of DiI in the peripheral dorsal retina at P8 labeled a single TZ in the lateral SC in P10 L1(Y1229H) mice. L, Lateral; M, medial; A, anterior; P, posterior; D, dorsal; V, ventral; N, nasal; T, temporal.

An EphB1-expressing subset of VT axons normally project ipsilaterally because of ephrinB2/EphB1-dependent axon divergence at the optic chiasm (Williams et al., 2003). To determine whether L1Y1229H) RGC axons were impaired for guidance at the optic chiasm, DiI crystals were inserted onto the optic disk of one eye to label contralaterally and ipsilaterally projecting axons in mutant and WT littermates (P10). As shown in whole mounts, most labeled RGC axons in the optic nerve crossed the midline at the optic chiasm to the contralateral optic tract and a small ipsilateral projection was observed in both WT and L1(Y1229H) mutants (Fig. 2*F*). RGC axons in the optic nerve and optic tract exhibited a similar degree of fasciculation in WT and mutants. Direct measurement of the diameter of the optic nerve at a position 400 μm from the midline of the optic chiasm showed no significant differences (*t* test, two-tailed) in means for WT (338 $\pm$ 27 μm; $n = 4$) and L1(Y1229H) mutants (402 $\pm$ 24 μm; $n = 6$; $p \leq 0.05$). The mean width of the optic chiasm measured at the midline was also not significantly different for WT (873 $\pm$ 37 μm; $n = 4$) and L1(Y1229H) mutants (920 $\pm$ 74 μm; $n = 6$). The mean width of the optic tract measured 100 μm posterior to the midline was also the same for WT (645 $\pm$ 76 μm; $n = 4$) and L1(Y1229H) mutants (691 $\pm$ 82 μm; $n = 6$), as was the diameter

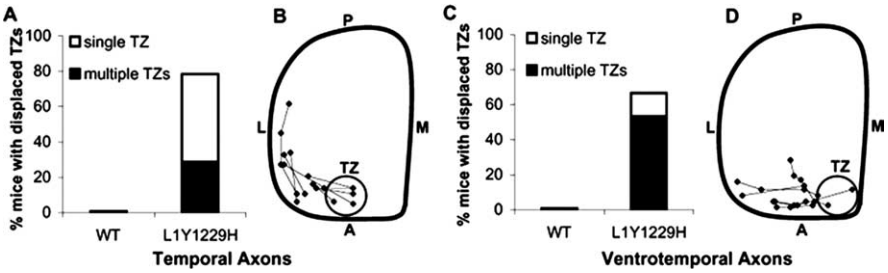

Figure 4. Displacement of termination zones of RGC axons in L1(Y1229H) mutant mice. ***A***, Percentage of mice with displaced TZs in the SC after temporal retinal injections at P10–P12. ***B***, Schematic representation of the location of TZs after temporal retinal injections in L1(Y1229H) mutant mice at P10. The centers of TZs and eTZs from mutant mice ($n = 10$) are marked and connected. Range of location of TZs of WT mice in the anteromedial SC is depicted by the gray circle. ***C***, Percentage of mutant mice with displaced TZs after ventrotemporal retinal injections at P10. ***D***, Schematic representation of the aberrant eTZs after ventrotemporal retinal injections in mutant mice ($n = 6$). L, Lateral; M, medial; A, anterior; P, posterior.

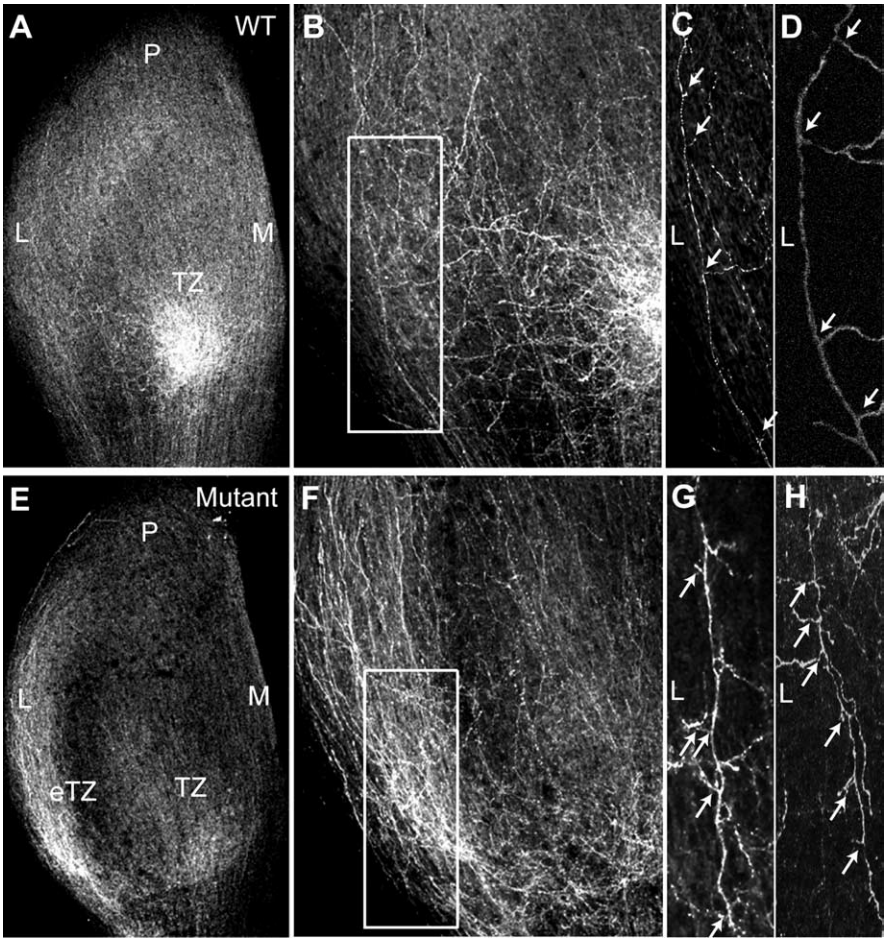

Figure 5. Abnormal directional branch extension in WT and L1(Y1229H) mutant mice at P2. ***A***, ***B***, Labeling of RGC axons at P2 after focal injections of DiI in the ventrotemporal retina of WT mice show interstitial branches extending toward the nascent TZ in the anteromedial SC. ***C***, ***D***, Most of the branches extending from axons that navigate lateral to the future TZ are oriented medially as shown in a higher magnification of the boxed area in B from confocal *z*-stacks (arrows). ***E***, ***F***, DiI labeling of VT axons in the SC of L1(Y1229H) mice at P2 reveal an accumulation at an inappropriate ectopic TZ (eTZ) as well as at a more appropriate future TZ. ***G***, ***H***, Many interstitial branches of mutant VT axons are abnormally oriented toward the lateral SC, as shown in a higher magnification of the boxed area in ***F*** from *z*-stacks (arrows). M, Medial; L, lateral; P, posterior.

of the ipsilateral projection in WT (359 ± 30 μm; $n = 4$) and mutant (360 ± 32 μm; $n = 6$). Thus, the loss of L1 binding to ankyrin did not impair the ability of RGC axons to cross the optic chiasm correctly or fasciculate, hence, mistargeting of L1(Y1229H) axons to the lateral SC is unlikely to be attributable to defects in guidance at the chiasm.

In summary, temporal and ventrotemporal retinal axons of L1(Y1229H) mutant mice misprojected primarily along the mediolateral SC axis to inappropriate lateral positions, with only slight anteroposterior malpositioning. These results suggested that L1 association with the actin cytoskeleton through ankyrin is important in the mechanism of topographic mapping of RGC axons to contralateral targets along the mediolateral axis of the SC.

Misdirected interstitial branching of retinal axons in developing L1(Y1229H) mutant mice

To investigate the mechanism responsible for the formation of ectopic termination zones of RGC axons in the L1(Y1229H) SC, the development of the contralateral retinocollicular projection was analyzed in mutants and WT littermates at P2–P3. Embryonic RGC axons at E14 enter the SC at its anterior border and grow posteriorly across the SC until covering it completely around P0, thus overshooting their future TZ location along the anteroposterior axis (McLaughlin and O'Leary, 2005). Around P2, the overshooting RGC axons branch interstitially with a mediolateral bias for the topographically correct site of their future TZ. The direction of interstitial axon branching is mediated by a balance of attractant and repellent forces including the high medial to low lateral gradients of ephrinB1 and Wnt3 in the SC (Hindges et al., 2002; McLaughlin et al., 2003b; Schmitt et al., 2006). As the TZ matures, the overshooting axon is then remodeled.

To investigate the hypothesis that the L1–ankyrin interaction influences ephrinB1-dependent interstitial branching, RGC axons in the SC and their developing interstitial branches at P2–P3 were analyzed after DiI injections into the VT retina at P1–P2. In WT mice, DiI labeling (Fig. 5*A–D*) showed labeled VT axons entering the SC spread along the mediolateral SC axis with a bias toward the position of their future correct anteromedial TZ (Fig. 5*A*). Interstitial branches extending from RGC axon shafts were preferentially oriented toward the future TZ. Branches extending from axons navigating in the lateral SC were oriented medially (Fig. 5*C*,*D*, arrowheads), whereas branches extending from axons in the medial SC were oriented laterally. In L1(Y1229H) mutant mice (Fig. 5*E–H*), DiI labeling of VT RGC axons at P1–P2 revealed that most branches extending from the shafts of axons navigating in the lateral SC were directed laterally; i.e., away from the correct termination site (Fig. 5*G*,*H*, arrowheads). In some mutants, a developing ectopic TZ was observed between the axons in the lateral SC (Fig. 5*E*).

To quantitatively evaluate branch orientation of VT axons in L1(Y1229H) and WT mice at P2–P3, the SC was divided into three bins along the mediolateral axis relative to the emerging TZ: lateral to TZ, within TZ, and medial to TZ (Fig. 6). The total number of labeled axons and branches was counted, and medial or lateral branch orientation was recorded for each bin (Fig. 6*A*,*B*). The results were expressed as a DC, which was calculated for each subject in each of the bins, as the difference in number of medial and lateral branches, divided by the total number of branches, as defined in (Hindges et al., 2002). A positive DC indicated more medial than lateral branches, whereas a negative DC indicated more lateral than medial branches. Analysis of RGC axons in the SC at P2–P3 after DiI injection into the VT retina confirmed that in WT mice ($n = 8$) interstitial axon branches were preferentially oriented toward the future TZ along the mediolateral axis. The majority of branches in the lateral bin were oriented medially toward the TZ, branches of axons in the TZ bin were largely unbiased, and the majority of branches in the medial bin were oriented laterally toward the TZ (Fig. 6*B*). In contrast, VT axons of L1(Y1229H) mutants ($n = 10$) in the lateral bin were oriented laterally with respect to the TZ, whereas branches of axons in the TZ and medial bins were normally oriented.

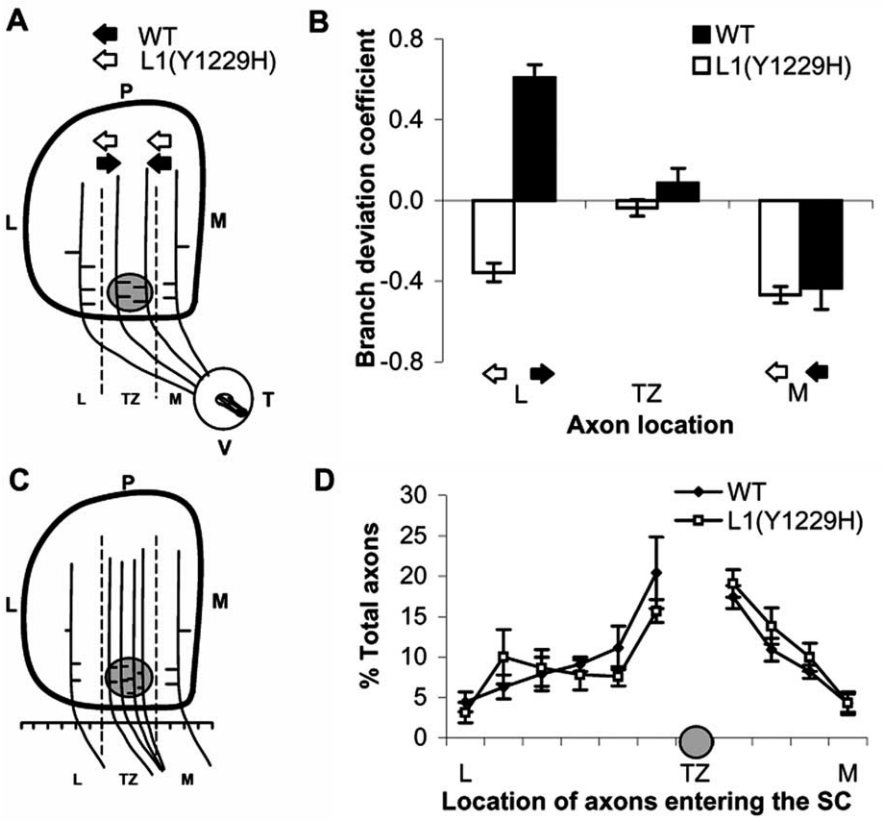

Figure 6. Branching and axonal positioning patterns in the SC of WT and L1(Y1229H) mice at P2. ***A***, Schematic representation of directed branch extension along the mediolateral axis. The SC was divided in three bins [lateral (L), TZ, medial (M)] separated by dash lines, in relation to the forming TZ (gray circle). The orientation of each branch was recorded and graphed by bin. ***B***, Distribution of branches in P2–P3 WT and L1(Y1229H) mutant mice after VT retinal injections. Arrows represent the direction of the branching preference in each region. The results were expressed as a branch directional coefficient as described (Hindges et al., 2002), calculated for each subject for each of the three bins of the SC as the difference in the number of medially oriented branches minus the number of laterally oriented branches, divided by the total number of branches. ***C***, Schematic representation of RGC axon positioning in the SC in WT and mutant mice. The SC was divided into 10 segments along the mediolateral axis at the anterior border, and all labeled RGC axons within each bin were counted and represented relative to the position of the developing TZ for each injection. ***D***, Distribution of labeled axons along the mediolateral SC axis (expressed as percentage of total) in L1(Y1229H) mice compared to WT littermates at P2, after VT retinal injections. Error bars indicate SEM.

The DCs were compared by a mixed ANOVA for WT ($n = 8$ mice; 437 branches) and L1(Y1229H) mutants ($n = 10$ mice; 754 branches). The statistical analysis revealed a significant main effect of genotype ($F_{(1,16)} = 75.28$; $p < 0.00001$), demonstrating that branch orientation in L1(Y1229H) mice was different from WT. Analysis of the interaction between bin and genotype indicated a significant difference in branching of WT and mutant axons in the lateral bin ($F_{(2,32)} = 29.99$; $p < 0.00001$), but not the medial bin ($t_{(16)} = 0.32$; $p = 0.75$). Analyses also showed no significant difference within the TZ ($t_{(16)} = 1.55$; $p = 0.14$), where the DC was not significantly different from zero for either genotype (WT, $t_{(7)} = 1.18$, $p = 0.28$; L1(1229H) mice, $t_{(9)} = 0.92$, $p = 0.38$).

In summary, these results suggested that disruption of L1 association with ankyrin resulted in a decrease in the ability of interstitial branches of VT axons to be attracted medially toward an increasing ephrinB1 gradient, similar to that seen in mice deficient in EphB2/EphB3 receptors (Hindges et al., 2002), whereas repellent guidance of medial axons away from the ephrinB1 gradient was preserved.

To evaluate whether disruption of the L1–ankyrin interaction resulted in different patterns of axonal entrance into the SC, the distribution of DiI-labeled VT axons entering the SC was evaluated at P2-P3, after retinal injections at P1. For each mouse the entrance zone into the SC was divided into 10 equal bins: four bins located medial to the TZ, and six bins lateral to the TZ. The percentage of axons entering the SC in each bin was scored for each subject (Fig. 6*C*), and averaged over groups (Fig. 6*D*). The distribution of axons (expressed as percentage of total for each bin) for WT ($n = 6$ mice; 291 axons) and L1(Y1229H) mice ($n = 9$ mice; 442 axons) was then analyzed by a mixed ANOVA. The analysis revealed no significant differences between WT and L1(Y1229H) mice ($F_{(9,117)} = 0.66$; $p > 0.75$). As expected, there was a significant effect of the entry position of VT axons in both WT and mutant mice ($F_{(9,117)} = 10.54$; $p < 0.0001$), such that more axons entered the SC in the vicinity of the TZ, decreasing medially and laterally. Thus, laterally displaced ectopic TZs in the L1(Y1229H) mutant were probably not caused by impaired axonal entrance into the SC.

L1–ankyrin binding is required for ephrinB1-induced modulation of cell adhesion

Mice deficient in both EphB2 and EphB3 display topographically aberrant projections along the mediolateral SC axis resulting in laterally displaced ectopic TZs and disrupted branch extension (Hindges et al., 2002). The strong similarity of mapping defects in L1(Y1229H) mice and EphB2/EphB3 knock-out mice suggested that the lateral displacement of temporal and VT RGC axons in L1(Y1229H) mice might be caused by altered responsiveness to ephrinB1-mediated attraction to medial positions. If dynamic

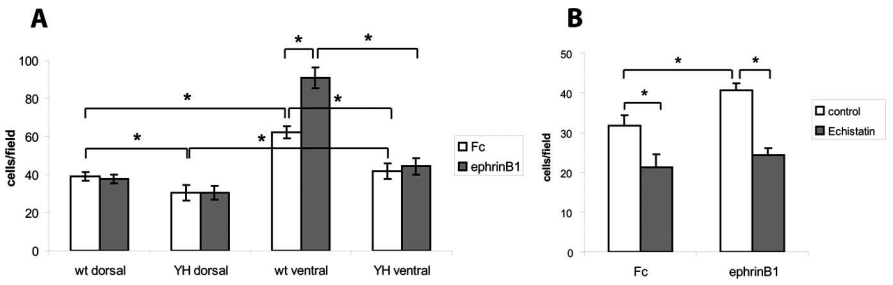

Figure 7. L1/ankyrin interaction promotes ephrinB1-stimulated, integrin-mediated retinal cell adhesion. ***A***, Retinal cell adhesion to fibronectin was quantified by determining the mean number of cells per field from three or more independent assays. Adhesion of WT ventral retinal cells to fibronectin was greater than WT dorsal retinal cells, and was stimulated by ephrinB1-Fc. Adhesion of L1(Y1229H) ventral retinal cells was lower than WT ventral cells and was not stimulated by ephrinB1-Fc. Total cell numbers were as follows: WT ventral retina, $n = 100$; WT dorsal retina, $n = 80$; LIYH ventral retina, $n = 100$; LIYH dorsal retina, $n = 60$. $*p < 0.05$, statistical significance was analyzed using the two-tailed *t* test. ***B***, Echistatin peptide (5 μg/ml), an inhibitor of RGD-binding integrins, decreased adhesion of WT ventral retinal cells to fibronectin-coated dishes treated with preclustered ephrinB1-Fc fusion protein (1 μg/ml) or Fc control protein. A representative experiment (from a total of 3 experiments) is shown with $n = 20$ cells per condition. Statistical significance was analyzed using the two-tailed *t* test, $*p < 0.05$.

modulation of adhesion is a factor in these axonal guidance responses, loss of ankyrin binding might decrease L1-dependent adhesion required for ephrinB/EphB function, thus reducing the ability of interstitial branches to be attracted medially. Integrins are important players in cell adhesion (Brakebusch and Fassler, 2005) and are known to interact with other guidance receptors and adhesion molecules, including L1 (Silletti et al., 2000; Mechtersheimer et al., 2001; Thelen et al., 2002). Moreover, β1 integrins contribute to retinotectal mapping in *Xenopus* (Stone and Sakaguchi, 1996), and EphrinB1/EphB2 signaling alters integrin-dependent cell adhesion in several cell systems (Miao et al., 2005).

Differential dorsoventral responses (branching or outgrowth) of RGC axons to lateral-medial guidance cues are difficult to demonstrate *in vitro*, most likely because such assays are more sensitive to repellent signals, as discussed previously (Hindges et al., 2002). However, cell adhesion assays have revealed differential adhesion of ventral vs dorsal retinal cells to ephrinB1 (Holash and Pasquale, 1995). To evaluate whether the differences in the interstitial branch extension of ventral versus dorsal retinal axons in the SC may be a result of different adhesive properties, we investigated the adhesion of retinal cells to fibronectin, a substrate normally present along radial glia in the tectum/SC (Stettler and Galileo, 2004). WT ventral retinal cells, which express higher levels of EphB2 and EphB3 than dorsal cells (Hindges et al., 2002), exhibited significantly enhanced adhesion to fibronectin when compared with dorsal retinal cells, reflecting intrinsic differences in their adhesive mechanisms (Fig. 7*A*). Furthermore, adhesion of WT ventral cells was stimulated by addition of ephrinB1-Fc fusion protein (1 μg/ml, preclustered with goat anti-human IgG) to activate EphB receptors, to a significantly greater extent than adhesion of cells treated with preclustered nonimmune IgG. In contrast to ventral retinal cells, no effect of ephrinB1-Fc was seen on adhesion of dorsal retinal cells. To demonstrate that ephrinB1-stimulated adhesion of ventral retinal cells was mediated by RGD-dependent integrins, adhesion of WT retinal cells to fibronectin was examined in the presence of echistatin, a competitive disintegrin peptide that blocks RGD-binding integrins (Musial et al., 1990). Echistatin significantly reduced basal adhesion of ventral retinal cells and completely abolished the stimulating effect of ephrinB1 on adhesion ($p < 0.01$) (Fig. 7*B*). Axons and growth cones were not seen because of the short term nature of the assay. Thus, ephrinB1-stimulated adhesion of ventral retinal cells to fibronectin appeared to be mediated by RGD integrins.

To determine whether ankyrin binding to L1 potentiated adhesion of retinal cells to fibronectin, and whether this potentiation was also regulated by ephrinB/EphB, dissociated cells from the dorsal or ventral retina of WT or L1Y1229H mice were assayed for adhesion to fibronectin in the presence of preclustered ephrinB1-Fc or nonimmune IgG. Both dorsal and ventral cells from L1Y1229H mice exhibited significantly less adhesion than corresponding WT retinal cells. Furthermore, ventral retinal cells of L1(Y1229H) mutants were more adherent than dorsal cells, and their adhesion was not altered by ephrinB1 stimulation (Fig. 7*A*).

These results indicate that L1 linkage to the cytoskeleton through ankyrin contributed to ephrinB/EphB-stimulated adhesion, and thus it may be important in topographic mapping of ventral retinal axons to appropriate targets through medially directed branch extension toward the increasing ephrinB/EphB-stimulated adhesion.

Discussion

The L1(Y1229H) mutant is the first example of a point mutation in an adhesion molecule that disrupts topographic axon targeting, and is a model for the human L1 syndrome of mental retardation and optic atrophy. Analysis of the L1(Y1229H) mice deficient in ankyrin binding has revealed that L1 linkage to the actin cytoskeleton is an essential component in the mechanism by which axons from the dorsoventral axis of the retina are mapped to the mediolateral axis of the SC. Loss of L1–ankyrin binding caused ventral retinal axons to terminate abnormally in laterally displaced ectopic TZs, and to inhibit extension of interstitial branches directed medially toward the increasing ephrinB1 gradient in the SC. Furthermore, L1–ankyrin binding was required for ephrinB1-promoted adhesion of dissociated ventral retinal cells to fibronectin substrates *in vitro*. Our study proposes that the mediolateral gradient of ephrinB1 attracts interstitial branches of RGC axons toward the midline of the SC through adhesive interactions enhanced by L1 linkage to the actin cytoskeleton.

Comparison of the phenotype of L1(Y1229H) mice with the L1 null mutant (Demyanenko and Maness, 2003) suggests that ankyrin-dependent and ankyrin-independent functions of L1 work in parallel to facilitate mapping along both SC axes. In contrast to L1(Y1229H) mutants, which showed striking mediolateral targeting defects and small anteroposterior errors, L1 knock-out mice exhibited prominent errors along both axes (Demyanenko and Maness, 2003). The anteroposterior mapping errors in L1 null mutants appeared to result from interstitial axon branching malpositioned inappropriately posterior to the normal TZ, as well as to lack of remodeling of the overshooting axon, both of which likely reflect defective responses to ephrinA/EphA guidance. Because of the much smaller posterior displacement of axon in L1(Y1229H) mice, this deviation could be attributable to competitive interactions with other mutant axons that are displaced laterally within the SC curvature. The phenotypes suggest that ankyrin-dependent functions, which are deleted in both L1(Y1229H) and L1 null mutants, regulate branch orientation and/or stabilization important for ephrinB1/EphB-guided me-

diolateral targeting (Hindges et al., 2002; McLaughlin et al., 2003a,b), whereas ankyrin-independent functions, which are deleted in L1-minus but not in L1(Y1229H) mutants, regulate interstitial branching and axon remodeling mediated by ephrinA/EphA-guided anteroposterior targeting (Yates et al., 2001).

The phenotype of L1(Y1229H) mice was strikingly similar to that of EphB2/EphB3-deficient or EphB2$^{ki/ki}$ forward signaling-deficient mice, which show lateral shifts (and a smaller posterior shift) of VT axon TZs and a decrease in medially directed branches (Hindges et al., 2002). Medially directed branching is thought to be the effect of a low lateral to high medial gradient of ephrinB1 in the SC on ventral RGC axons expressing high levels of EphB2/EphB3 (Hindges et al., 2002; McLaughlin et al., 2003a,b). L1–ankyrin interaction at the FIGQY sequence appears to promote medial branch extension and/or stabilization, which occurs through synapse formation (Meyer and Smith, 2006; Ruthazer et al., 2006), rather than to function in the presorting of axons at the entrance to the SC. Studies on the *Drosophila* L1 homolog Neuroglian, whose FIGQY sequence is responsible for ankyrin binding and cell adhesion (Hortsch et al., 1998), show that this sequence is crucial for the formation of central synapses (Godenschwege et al., 2006). L1–ankyrin function did not seem to be involved in propagating a repellent counterforce, such as that mediated by Wnt/Ryk signaling (Schmitt et al., 2006), as the formation of lateral interstitial branches in L1(Y1229H) mutant axons was unaffected. Furthermore, L1–ankyrin binding was not necessary for axon growth per se, as shown by the normal extension of contralateral and ipsilateral RGC axons along the optic nerve and tract of L1(Y1229H) mice. This agrees with the minimal inhibitory effects on neurite growth of cerebellar neurons expressing L1 cytoplasmic domain truncations encompassing the FIGQY sequence (Cheng et al., 2005). In ankyrin B null mutant mice, the optic tract also forms but degenerates postnatally, suggesting that ankyrin B recruitment to L1 family members contributes to stabilization in the retinocollicular system (Scotland et al., 1998). Because most ankyrin B null mice die perinatally, it is not feasible to map the location of final TZs, which could verify the role of ankyrin B in L1-mediated retinocollicular targeting. We cannot exclude that the Tyr1229His mutation in L1 might also alter binding of the clathrin adaptor AP2 or ERM proteins to the cytoplasmic domain, however, these proteins are known to bind to distinct sites (Kamiguchi et al., 1998; Dickson et al., 2002; Cheng et al., 2005). Although doublecortin has been reported to bind to the phosphorylated FIGQY motif (Kizhatil et al., 2002), this microtubule-associated protein did not coimmunoprecipitate with L1 from mouse brain (E15.5–17.5) and was expressed and localized with a similar pattern in WT and L1(Y1229H) brain (our unpublished observation).

A mechanism for mediolateral targeting has been described in which ephrinBs exert concentration-dependent attractive and repulsive forces on axons by modulating cell-substrate adhesion, causing axons to terminate at positions within the ephrinB gradient where adhesion is optimal (McLaughlin et al., 2003b; Flanagan, 2006). Our results suggest that L1–ankyrin association contributes to ephrinB1/EphB-induced extension and/or stabilization of medially directed branches of ventral RGC axons expressing high levels of EphB receptors. This idea is consistent with the behavior of dissociated retinal neurons in which L1–ankyrin binding contributed to ephrinB1-stimulated adhesion of ventral but not dorsal retinal cells through RGD-binding integrins. Cell adhesion might involve different mechanistic components, but our results are consistent with a role for adhesion in ephrinB1-mediated RGC branch attraction. L1 is known to associate with β1 integrins through the L1 extracellular domain and to potentiate RGD integrin-dependent cell adhesion in non-neuronal cells ((Silletti et al., 2000; Mechtersheimer et al., 2001; Thelen et al., 2002; Panicker et al., 2006). EphrinB/EphB stimulation in non-neuronal cells has also been shown to enhance cell adhesion through β1 integrins (Gu and Park, 2001; Huynh-Do et al., 2002; Matsuoka et al., 2005; Miao et al., 2005). *In vivo*, ephrinB1 (Hindges et al., 2002) and fibronectin (Stettler and Galileo, 2004) are present on radial glia within the superficial layers of the tectum/SC where RGC axons travel, and thus are in position to engage EphB receptors and integrins. Although L1 is localized on RGC axons and in deeper layers of the SC (Lemmon and McLoon, 1986; Yamagata et al., 1995; Demyanenko and Maness, 2003), little if any is present in the upper layers of the SC (Lyckman et al., 2000), thus homophilic L1 binding is unlikely to influence RGC axon targeting. However, other L1 binding partners such as TAG-1, contactin, or ALCAM may be present in the SC, and could contribute to heterophilic interactions. Although no dorsoventral or nasotemporal gradient of L1 protein was seen in the early postnatal mouse retina (present study) (Demyanenko and Maness, 2003), the graded expression of Eph receptors interacting with L1 could account for the specific effects of the L1(Y12229H) mutation on medially oriented branching. Moreover, the results of Williams et al. (2006) and our own results do not show a difference in L1 expression in the VT region of the retina at E14.5 or E17.5; thus, VT axons are most likely affected by the loss of L1/ankyrin binding because of functional interaction with the high levels of EphB receptors.

Reversible phosphorylation of L1 on Tyr1229 inhibits ankyrin binding (Garver et al., 1997) downstream of ERK MAP kinase (Whittard et al., 2006), but the enzyme that directly phosphorylates L1 has not been identified. Although overexpression of EphB2 and L1 in a glioblastoma cells line causes L1 phosphorylation on an unidentified tyrosine residue (Zisch et al., 1997), it is unlikely that this involves L1Tyr1229, because such phosphorylation would decrease ankyrin binding and thereby reduce adhesion after ephrinB1 stimulation, which is in contrast to our results. In addition L1 did not coimmunoprecipitated with EphB2 or EphB3 from SC extracts (P1–P2).

These findings suggest that L1–ankyrin interactions may contribute to the development of adhesive force necessary to promote ephrinB1-induced medial extension of interstitial branches of retinal axons that lead to appropriately positioned TZs. In accord with this idea, ankyrin binding to L1 family members promotes adhesion (Tuvia et al., 1997) and fosters stationary behavior of cells by inhibiting retrograde actin flow (Hortsch et al., 1998; Gil et al., 2003). Analogous to the proposed function of L1–ankyrin interactions in retinotopic mapping, binding of ankyrin to neurofascin is involved in targeting of basket cell axons in the cerebellum to the Purkinje cell axon initial segment (Ango et al., 2004). Thus, linkage of L1 family molecules to the cytoskeleton through ankyrin binding may be a general principle for modulating adhesion essential to the function of many axon guidance systems that control neuronal wiring throughout the nervous system.

References

Ango F, di Cristo G, Higashiyama H, Bennett V, Wu P, Huang ZJ (2004) Ankyrin-based subcellular gradient of neurofascin, an immunoglobulin family protein, directs GABAergic innervation at Purkinje axon initial segment. Cell 119:257–272.

Birgbauer E, Cowan CA, Sretavan DW, Henkemeyer M (2000) Kinase independent function of EphB receptors in retinal axon pathfinding to the optic disc from dorsal but not ventral retina. Development 127:1231–1241.

Brakebusch C, Fassler R (2005) beta 1 integrin function *in vivo*: adhesion, migration and more. Cancer Metastasis Rev 24:403–411.

Burgoon MP, Grumet M, Mauro V, Edelman GM, Cunningham BA (1991) Structure of the chicken neuron-glia cell adhesion molecule, Ng-CAM: origin of the polypeptides and relation to the Ig superfamily. J Cell Biol 112:1017–1029.

Chan W, Kordeli E, Bennett V (1993) 440-kD ankyrinB: structure of the major developmentally regulated domain and selective localization in unmyelinated axons. J Cell Biol 123:1463–1473.

Cheng L, Itoh K, Lemmon V (2005) L1-mediated branching is regulated by two ezrin-radixin-moesin (ERM)-binding sites, the RSLE region and a novel juxtamembrane ERM-binding region. J Neurosci 25:395–403.

Davis JQ, Bennett V (1994) Ankyrin binding activity shared by the neurofascin/L1/NrCAM family of cell adhesion molecules. J Biol Chem 269:27163–27166.

Demyanenko G, Tsai A, Maness PF (1999) Abnormalities in neuronal process extension, hippocampal development, and the ventricular system of L1 knockout mice. J Neurosci 19:4907–4920.

Demyanenko GP, Maness PF (2003) The L1 cell adhesion molecule is essential for topographic mapping of retinal axons. J Neurosci 23:530–538.

Dickson TC, Mintz CD, Benson DL, Salton SR (2002) Functional binding interaction identified between the axonal CAM L1 and members of the ERM family. J Cell Biol 157:1105–1112.

Drescher U, Kremoser C, Handwerker C, Löschinger J, Noda M, Bonhoeffer F (1995) In vitro guidance of retinal ganglion cell axons by RAGS, a 25 kDa tectal protein related to ligands for Eph receptor tyrosine kinases. Cell 82:359–370.

Feldheim DA, Kim YI, Bergemann AD, Frisen J, Barbacid M, Flanagan JG (2000) Genetic analysis of ephrin-A2 and ephrin-A5 shows their requirement in multiple aspects of retinocollicular mapping [see comments]. Neuron 25:563–574.

Feldheim DA, Nakamoto M, Osterfield M, Gale NW, DeChiara TM, Rohatgi R, Yancopoulos GD, Flanagan JG (2004) Loss-of-function analysis of EphA receptors in retinotectal mapping. J Neurosci 24:2542–2550.

Felding-Habermann B, Silletti S, Mei F, Siu CH, Yip PM, Brooks PC, Cheresh DA, O'Toole TE, Ginsberg MH, Montgomery AM (1997) A single immunoglobulin-like domain of the human neural cell adhesion molecule L1 supports adhesion by multiple vascular and platelet integrins. J Cell Biol 139:1567–1581.

Flanagan JG (2006) Neural map specification by gradients. Curr Opin Neurobiol 16:59–66.

Garver TD, Ren Q, Tuvia S, Bennett V (1997) Tyrosine phosphorylation at a site highly conserved in the L1 family of cell adhesion molecules abolishes ankyrin binding and increases lateral mobility of neurofascin. J Cell Biol 137:703–714.

Gil OD, Sakurai T, Bradley AE, Fink MY, Cassella MR, Kuo JA, Felsenfeld DP (2003) Ankyrin binding mediates L1CAM interactions with static components of the cytoskeleton and inhibits retrograde movement of L1CAM on the cell surface. J Cell Biol 162:719–730.

Godenschwege TA, Kristiansen LV, Uthaman SB, Hortsch M, Murphey RK (2006) A conserved role for *Drosophila* Neuroglian and human L1-CAM in central-synapse formation. Curr Biol 16:12–23.

Gu C, Park S (2001) The EphA8 receptor regulates integrin activity through p110gamma phosphatidylinositol-3 kinase in a tyrosine kinase activity-independent manner. Mol Cell Biol 21:4579–4597.

Hansen MJ, Dallal GE, Flanagan JG (2004) Retinal axon response to ephrin-as shows a graded, concentration-dependent transition from growth promotion to inhibition. Neuron 42:717–730.

Hindges R, McLaughlin T, Genoud N, Henkemeyer M, O'Leary DD (2002) EphB forward signaling controls directional branch extension and arborization required for dorsal-ventral retinotopic mapping. Neuron 35:475–487.

Holash JA, Pasquale EB (1995) Polarized expression of the receptor protein tyrosine kinase Cek5 in the developing avian visual system. Dev. Biol 172:683–693.

Hortsch M, Homer D, Malhotra JD, Chang S, Frankel J, Jefford G, Dubreuil RR (1998) Structural requirements for outside-in and inside-out signaling by *Drosophila* neuroglian, a member of the L1 family of cell adhesion molecules. J Cell Biol 142:251–261.

Huynh-Do U, Vindis C, Liu H, Cerretti DP, McGrew JT, Enriquez M, Chen J, Daniel TO (2002) Ephrin-B1 transduces signals to activate integrin-mediated migration, attachment and angiogenesis. J Cell Sci 115:3073–3081.

Jenkins SM, Kizhatil K, Kramarcy NR, Sen A, Sealock R, Bennett V (2001) FIGQY phosphorylation defines discrete populations of L1 cell adhesion molecules at sites of cell-cell contact and in migrating neurons. J Cell Sci 114:3823–3835.

Kalil K, Dent EW (2005) Touch and go: guidance cues signal to the growth cone cytoskeleton. Curr Opin Neurobiol 15:521–526.

Kamiguchi H, Long KE, Pendergast M, Schaefer AW, Rapoport I, Kirchhausen T, Lemmon V (1998) The neural cell adhesion molecule L1 interacts with the AP-2 adaptor and is endocytosed via the clathrin-mediated pathway. J Neurosci 18:5311–5321.

Kenwrick S, Watkins A, Angelis ED (2000) Neural cell recognition molecule L1: relating biological complexity to human disease mutations. Hum Mol Genet 9:879–886.

Kizhatil K, Wu YX, Sen A, Bennett V (2002) A new activity of doublecortin in recognition of the phospho-FIGQY tyrosine in the cytoplasmic domain of neurofascin. J Neurosci 22:7948–7958.

Kunimoto M, Otto E, Bennett V (1991) A new 440-kd isoform is the major ankyrin in neonatal brain. J Cell Biol 115:1319–1331.

Lemke G, Reber M (2005) Retinotectal mapping: new insights from molecular genetics. Annu Rev Cell Dev Biol 21:551–580.

Lemmon V, McLoon SC (1986) The appearance of an L1-like molecule in the chick primary visual pathway. J Neurosci 6:2987–2994.

Lyckman AW, Moya KL, Confaloni A, Jhaveri S (2000) Early postnatal expression of L1 by retinal fibers in the optic tract and synaptic targets of the Syrian hamster. J Comp Neurol 423:40–51.

Maness PF, Schachner M (2007) Neural recognition molecules of the immunoglobulin superfamily: signaling transducers of axon guidance and neuronal migration. Nat Neurosci 10:19–26.

Mann F, Harris WA, Holt CE (2004) New views on retinal axon development: a navigation guide. Int J Dev Biol 48:957–964.

Matsuoka H, Obama H, Kelly ML, Matsui T, Nakamoto M (2005) Biphasic functions of the kinase-defective Ephb6 receptor in cell adhesion and migration. J Biol Chem 280:29355–29363.

McLaughlin T, O'Leary DD (2005) Molecular gradients and development of retinotopic maps. Annu Rev Neurosci 28:327–355.

McLaughlin T, Hindges R, O'Leary DD (2003a) Regulation of axial patterning of the retina and its topographic mapping in the brain. Curr Opin Neurobiol 13:57–69.

McLaughlin T, Hindges R, Yates PA, O'Leary DD (2003b) Bifunctional action of ephrin-B1 as a repellent and attractant to control bidirectional branch extension in dorsal-ventral retinotopic mapping. Development 130:2407–2418.

Mechtersheimer S, Gutwein P, Agmon-Levin N, Stoeck A, Oleszewski M, Riedle S, Fogel M, Lemmon V, Altevogt P (2001) Ectodomain shedding of L1 adhesion molecule promotes cell migration by autocrine binding to integrins. J Cell Biol 155:661–673.

Meyer MP, Smith SJ (2006) Evidence from in vivo imaging that synaptogenesis guides the growth and branching of axonal arbors by two distinct mechanisms. J Neurosci 26:3604–3614.

Miao H, Strebhardt K, Pasquale EB, Shen TL, Guan JL, Wang B (2005) Inhibition of integrin-mediated cell adhesion but not directional cell migration requires catalytic activity of EphB3 receptor tyrosine kinase. Role of Rho family small GTPases. J Biol Chem 280:923–932.

Musial J, Niewiarowski S, Rucinski B, Stewart GJ, Cook JJ, Williams JA, Edmunds Jr LH (1990) Inhibition of platelet adhesion to surfaces of extracorporeal circuits by disintegrins. RGD-containing peptides from viper venoms. Circulation 82:261–273.

Needham LK, Thelen K, Maness PF (2001) Cytoplasmic domain mutations of the L1 cell adhesion molecule reduce L1- ankyrin interactions. J Neurosci 21:1490–1500.

Otto E, Kunimoto M, McLaughlin T, Bennett V (1991) Isolation and characterization of cDNAs encoding human brain ankyrins reveal a family of alternatively spliced genes. J Cell Biol 114:241–253.

Panicker AK, Buhusi M, Erickson A, Maness PF (2006) Endocytosis of beta1 integrins is an early event in migration promoted by the cell adhesion molecule L1. Exp Cell Res 312:299–307.

Ruthazer ES, Li J, Cline HT (2006) Stabilization of axon branch dynamics by synaptic maturation. J Neurosci 26:3594–3603.

Schmidt JT (2004) Activity-driven sharpening of the retinotectal projec-

tion: the search for retrograde synaptic signaling pathways. J Neurobiol 59:114–133.

Schmitt AM, Shi J, Wolf AM, Lu CC, King LA, Zou Y (2006) Wnt-Ryk signalling mediates medial-lateral retinotectal topographic mapping. Nature 439:31–37.

Scotland P, Zhou D, Benveniste H, Bennett V (1998) Nervous system defects of AnkyrinB (−/−) mice suggest functional overlap between the cell adhesion molecule L1 and 440-kD AnkyrinB in premyelinated axons. J Cell Biol 143:1305–1315.

Silletti S, Mei F, Sheppard D, Montgomery AM (2000) Plasmin-sensitive dibasic sequences in the third fibronectin-like domain of L1-cell adhesion molecule (CAM) facilitate homomultimerization and concomitant integrin recruitment. J Cell Biol 149:1485–1502.

Simon DK, O'Leary DD (1992) Influence of position along the medial-lateral axis of the superior colliculus on the topographic targeting and survival of retinal axons. Brain Res Dev Brain Res 69:167–172.

Stettler EM, Galileo DS (2004) Radial glia produce and align the ligand fibronectin during neuronal migration in the developing chick brain. J Comp Neurol 468:441–451.

Stone KE, Sakaguchi DS (1996) Perturbation of the developing *Xenopus* retinotectal projection following injections of antibodies against beta1 integrin receptors and N-cadherin. Dev Biol 180:297–310.

Thelen K, Kedar V, Panicker AK, Schmid RS, Midkiff BR, Maness PF (2002) The neural cell adhesion molecule L1 potentiates integrin-dependent cell migration to extracellular matrix proteins. J Neurosci 22:4918–4931.

Tuvia S, Garver TD, Bennett V (1997) The phosphorylation state of the FIGQY tyrosine of neurofascin determines ankyrin-binding activity and patterns of cell segregation. Proc Natl Acad Sci USA 94:12957–12962.

Whittard JD, Sakurai T, Cassella MR, Gazdoiu M, Felsenfeld DP (2006) MAP kinase pathway-dependent phosphorylation of the L1-CAM ankyrin binding site regulates neuronal growth. Mol Biol Cell 17:2696–2706.

Williams SE, Mann F, Erskine L, Sakurai T, Wei S, Rossi DJ, Gale NW, Holt CE, Mason CA, Henkemeyer M (2003) Ephrin-B2 and EphB1 mediate retinal axon divergence at the optic chiasm. Neuron 39:919–935.

Williams SE, Grumet M, Colman DR, Henkemeyer M, Mason CA, Sakurai T (2006) A role for Nr-CAM in the patterning of binocular visual pathways. Neuron 50:535–547.

Yamagata M, Herman JP, Sanes JR (1995) Lamina-specific expression of adhesion molecules in developing chick optic tectum. J Neurosci 15:4556–4571.

Yates PA, Roskies AL, McLaughlin T, O'Leary DD (2001) Topographic-specific axon branching controlled by ephrin-As is the critical event in retinotectal map development. J Neurosci 21:8548–8563.

Zisch AH, Stallcup WB, Chong LD, Dahlin-Huppe K, Voshol J, Schachner M, Pasquale EB (1997) Tyrosine phosphorylation of L1 family adhesion molecules: implication of the Eph kinase Cek5. J Neurosci Res 47:655–665.